OPEN ACCESS
Journal of Innovative Optical Health Sciences
Vol. 14, No. 2 (2021) 2050027 (11 pages)

DOI: 10.1142/S1793545820500273

World Scientific
www.worldscientific.com

Structured illumination microscopy based on asymmetric three-beam interference

Linyu Xu*, Yanwei Zhang†, Song Lang†, Hongwei Wang†,
Huijie Hu†, Jingkai Wang† and Yan Gong*,†,‡
*University of Science and Technology of China
Hefei, Anhui 230026, P. R. China

†Suzhou Institute of Biomedical Engineering and Technology
Chinese Academy of Sciences, Suzhou, Jiangsu 215163, P. R. China
‡18625160712@163.com

Received 28 April 2020
Accepted 30 August 2020
Published 17 October 2020

Structured illumination microscopy (SIM) is a rapidly developing super-resolution technology. It has been widely used in various application fields of biomedicine due to its excellent two- and three-dimensional imaging capabilities. Furthermore, faster three-dimensional imaging methods are required to help enable more research-oriented living cell imaging. In this paper, a fast and sensitive three-dimensional structured illumination microscopy based on asymmetric three-beam interference is proposed. An innovative time-series acquisition method is employed to halve the time required to obtain each raw image. A segmented half-wave plate as a substantial linear polarization modulation method is applied to the three-dimensional SIM system for the first time. Although it needs to acquire 21 raw images instead of 15 to reconstruct one super-resolution image, the SIM setup proposed in this paper is 30% faster than the traditional spatial light modulator-SIM (SLM-SIM) in imaging each super-resolution image. The related theoretical derivation, hardware system, and verification experiment are elaborated in this paper. The stable and fast 3D super-resolution imaging method proposed in this paper is of great significance to the research of organelle interaction, intercellular communication, and other biomedical fields.

Keywords: Super-resolution; structured illumination; asymmetric three-beam interference; three-dimensional imaging.

1. Introduction

In recent years, super-resolution imaging techniques that overcome optical diffraction limits have been rapidly developed.[1,2] Structured illumination microscopy (SIM) is one such super-resolution method. It has been demonstrated that by using spatially

‡Corresponding author.

structured illumination light to frequency-mix high-resolution information into the passband of the microscopy, SIM can double the lateral resolution of a conventional fluorescence microscope without any loss of light.[3–6] Compared with other super-resolution imaging methods, SIM presents certain advantages such as fast imaging speed, low phototoxicity, and a simple imaging system structure. In two-dimensional SIM, the sample is illuminated by two beams of light that interfere with each other to form a sinusoidal-varying light intensity pattern.[6] In 2008, Gustafsson *et al.* first conducted experiments to verify the three-dimensional resolution enhancement of the SIM system.[7] The fluorescent sample is illuminated with three mutually coherent beams of excitation light. Many researchers have obtained multi-polarization singularity vector light fields through three-beam and multi-beam interference methods, which may lead to novel concepts of SIM.[8–10]

Various research groups are actively developing three-dimensional imaging technology of SIM based on three-beam interference and applying it in a variety of biological studies.[11–19] Currently, large numerical aperture (NA) objectives are used for imaging in most laser SIM systems. The influence of the polarization state of the excitation light with the large NA objective is not negligible.[20] Moreover, it is necessary to adjust the polarization state of the excitation light in real-time to ensure high contrast of the interference fringes generated by the excitation light on the focal plane. The main methods of linear polarization direction modulation are: (1) controlling the phase delay of the liquid-crystal variable retarder together with a quarter-wave retarder[21]; (2) controlling the fast axis direction of the ferroelectric liquid-crystal wave plate combined with a quarter-wave plate[22]; (3) using a rotating polarizer; (4) using a quarter-wave plate with a segmented polarizer[23]; and (5) utilizing zero-order vortex half-wave retarder.[24] Liquid-crystal devices are utilized in methods (1) and (2), resulting in poor environmental stability. The modulation response time of method (3) is too long, leading to limiting the imaging speed. In method (4), 50% of the energy is lost. In method (5), the working bandwidth of the zero-order vortex half-wave plate is narrow, and it can only be used for monochrome imaging. These shortcomings of the polarization modulation methods impede the imaging ability of SIM systems, especially for three-dimensional imaging performance.

In 2008, a spatially variable retardation (SVR) plate was used to convert a linearly-polarized Gaussian beam to a radially- or an azimuthally-polarized Laguerre–Gaussian (LG) beams.[25] It led to a new polarization modulation method. Subsequently, Chen and co-workers applied it (called the segmented half-wave plates) for polarization modulation to a two-dimensional SIM system for the first time.[26] It was composed of six sectors of half-wave plates, each one with different orientation of the crystal's slow axis. This method did not introduce any moving parts, and it can avoid response time delay and has good environmental stability. However, the segmented half-wave plate cannot be used in a three-dimensional SIM system based on three-beam interference illumination because this method cannot modulate the polarization state of zero-order light.

In this paper, a new method named SIM based on asymmetric three-beam interference (ATI-SIM) is proposed to realize three-dimensional super-resolution imaging.

As the zero-order diffracted light is no longer used in the optical path, the segmented half-wave plate is used for the first time in 3D SIM imaging systems. Moreover, a new time-series acquisition method is adopted in ATI-SIM because of the characteristics of asymmetric three-beam interference illumination, resulting in a near-50% reduction in the acquisition time of each raw image. The feasibility of a three-dimensional SIM system based on asymmetric three-beam interference is verified through theoretical derivations and experiments.

2. Background Theory

In traditional three-dimensional SIM, ± 1 and 0 diffraction orders of the grating are refocused into the back focal plane of the objective. The three beams interfere with each other to generate an illumination fringe. However, the zeroth order of the diffracted beam cannot be utilized because the central position of the segmented half-wave plate is at the joint of six sector half-wave plates. In this study, an innovative method of structured illumination light using ATI between -2-, $+1$-, and $+2$-order diffracted lights is proposed.

In a linear-response fluorescence microscopic imaging system, the distribution of fluorescent emission is proportional to the illumination

intensity $I(\mathbf{r})$ and the density distribution of fluorescence dye $S(\mathbf{r})$. The intensity of the image and object satisfies the convolution relation in Eq. (1),

$$D(\mathbf{r}) = [I(\mathbf{r})S(\mathbf{r})] \otimes H(\mathbf{r}), \tag{1}$$

where $D(\mathbf{r})$ denotes the observed data, $H(\mathbf{r})$ denotes the point spread function, $\mathbf{r}$ is the coordinate vector, and $\otimes$ represents convolution.

Assume that the xy-plane is the sample plane and the z-axis is the vertical direction of the sample plane. The three beams can be expressed as follows, respectively:

$$E_1 = A_1 \exp\{-j[k(\mathbf{r}_{xy} \sin\theta_1 + z\cos\theta_1) + \phi_1]\}, \tag{2}$$

$$E_2 = A_2 \exp\{-j[k(\mathbf{r}_{xy} \sin\theta_2 + z\cos\theta_2) + \phi_2]\}, \tag{3}$$

$$E_3 = A_2 \exp\{-j[k(-\mathbf{r}_{xy} \sin\theta_2 + z\cos\theta_2) - \phi_2]\}, \tag{4}$$

where A_1 and A_2 denote the amplitudes, $\mathbf{r}_{xy}$ denotes the lateral coordinates, k represents the wave number, θ denotes the angle between the light and the optical axis, and ϕ_1 and ϕ_2 denote the phases of light. The three-light spots, corresponding to the -2, $+1$, and $+2$ diffraction orders of the spatial light modulator (SLM), are equally spaced on the back focal plane of the objective lens. Assume that on the back focal plane of the objective lens, the distance from the $+1$ spot to the center is x_1 and the distance from the $+2$ (-2) spot to the center is x_2 $(x_2 = 2x_1)$. In an optical microscopy system, $\frac{1}{\mathrm{NA}} = \frac{f}{x}$, where NA denotes the numerical aperture and f represents the focal length. It can be derived that

$$\sin\theta_2 = 2\sin\theta_1. \tag{5}$$

The intensity distribution of interference light on the sample plane is as shown in Eq. (6), where E^* represents the conjugate of E,

$$I(\mathbf{r}) = (E_1 + E_2 + E_3) \times (E_1^* + E_2^* + E_3^*). \tag{6}$$

Substituting Eqs. (2)–(4) into Eq. (6), it can be derived that

$$I(\mathbf{r}_{xy}, z) = \sum_m G_m(z) J_m(\mathbf{r}_{xy}), \tag{7}$$

where $m = 0, \pm1, \pm3, \pm4$; $J_m(\mathbf{r}_{xy})$ and $G_m(z)$ are the lateral and axial illumination intensities, respectively,

$$J_m(\mathbf{r}_{xy}) = \exp[j(2\pi \mathbf{p}_m \mathbf{r}_{xy} + \varphi_m)], \tag{8}$$

$$G_0(z) = A_1^2 + 2A_2^2, \tag{9}$$

$$G_{\pm1}(z) = A_1 A_2 \exp\left[-j\frac{zm}{|m|}(\cos\theta_1 - \cos\theta_2)\right], \tag{10}$$

$$G_{\pm3}(z) = A_1 A_2 \exp\left[j\frac{zm}{|m|}(\cos\theta_1 - \cos\theta_2)\right], \tag{11}$$

$$G_{\pm4}(z) = A_2^2, \tag{12}$$

where $\mathbf{p}_m$ is the lateral wave vector and φ_m is the phase shift.

For 3D SIM systems, the three-dimensional data are acquired via axial scanning of the object. The illumination pattern is fixed relative to the focal plane of the microscope, not in relation to the object. This means that $G_m(z)$ will depend on the difference coordinate of the objective lens and specimen frame. The measured data can be represented as the following convolution integral, which is suitable for three-dimensional SIM:

$$\begin{aligned} D(\mathbf{r}) &= \sum_m \int H(\mathbf{r} - \mathbf{r}') G_m(z - z') S(\mathbf{r}') J_m(\mathbf{r}'_{xy}) d\mathbf{r}' \\ &= \sum_m [(HG_m) \otimes (SJ_m)](\mathbf{r}). \end{aligned} \tag{13}$$

If D_m denote the mth term of the above sum, its Fourier transform can be obtained as follows:

$$\tilde{D}_m(\mathbf{k}) = [O(\mathbf{k}) \otimes \tilde{G}_m(\mathbf{k})] \cdot [\tilde{S}(\mathbf{k}) \otimes \tilde{J}_m(\mathbf{k})], \tag{14}$$

where $\mathbf{k}$ is the coordinate vector in the frequency domain and $O(\mathbf{k})$ is the optical transfer function (OTF) of the system,

$$\begin{aligned} \tilde{D}(\mathbf{k}) &= \sum_m \tilde{D}_m(\mathbf{k}) \\ &= \sum_m A_m O_m(\mathbf{k}) \exp(j\varphi_m) \tilde{S}(\mathbf{k} - m\mathbf{p}_{xy}), \end{aligned} \tag{15}$$

$$O_{\pm1}(\mathbf{k}) = O(\mathbf{k} + \mathbf{p}_z), \quad O_{\pm3}(\mathbf{k}) = O(\mathbf{k} - \mathbf{p}_z), \tag{16}$$

where $\mathbf{p}_{xy}$ and $\mathbf{p}_z$ are the lateral and axial spatial frequencies of illumination, respectively.

For an optical three-dimensional microscope system, the OTF support is a torus-like region [Fig. 1(a)]. The "hole" of the torus is the "missing cone" of information near the z-axis.[7] Therefore, the high-resolution tomographic images cannot be obtained via the conventional fluorescence microscopy. The principle behind SIM improving the resolution is to obtain the high-frequency information of samples by using illumination light of a specific structure. Three-dimensional super-resolution imaging is equivalent to finding an approach to detect

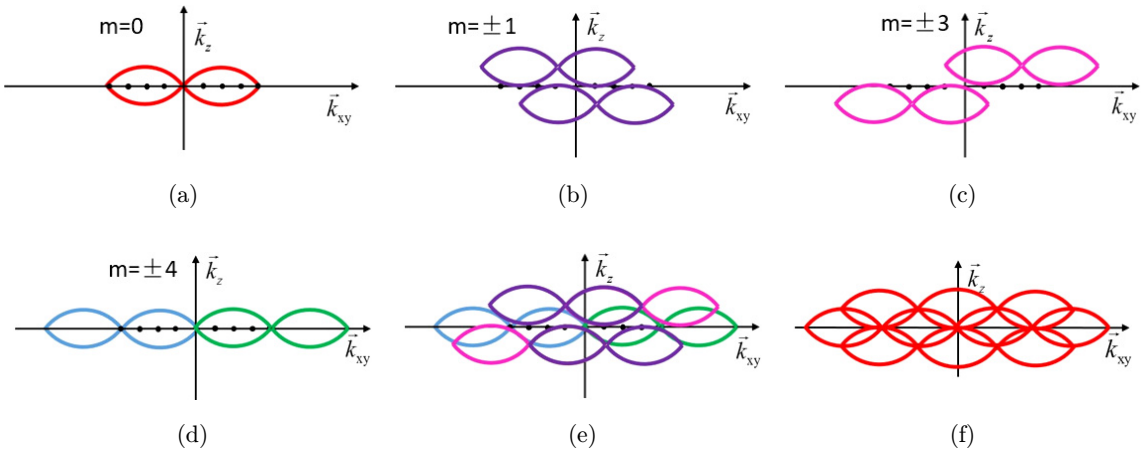

Fig. 1. Enlargement of the optical transfer function through structured illumination.

information from outside of the original observable region and solve the missing cone complication. The imaging distribution based on asymmetric three-beam interferometric illumination is illustrated in Eq. (15). A single raw data observation is a sum of seven components, each moved laterally by a distance $m\mathbf{P}_{xy}$ and filtered by a transfer function $O_m(\mathbf{K})$. Figures 1(b)–1(d) exhibit the detected sample information distributions in a three-dimensional frequency domain when m is equal to $\pm1, \pm3$, and ±4, respectively. The superposition of all the frequency components to construct the final super-resolution image of the SIM based on asymmetric three-beam interference is shown in Fig. 1(e). Moreover, the spectrum expansion diagram of the traditional three-dimensional SIM based on symmetrical three-beam interference is displayed in Fig. 1(f). It can be observed in Fig. 1(e) that the resolution in three dimensions is improved compared with Fig. 1(a). Therefore, the feasibility of three-dimensional SIM based on asymmetric three-beam interference illumination is theoretically verified. Moreover, it is indicated in Figs. 1(e) and 1(f) that the asymmetric three-beam interference illumination method can obtain the same lateral resolution and slightly lower axial resolution compared with the traditional three-beam interference method.

3. Materials and Methods

3.1. *Apparatus*

The implementation of SIM employed in this study is similar to the conventional laser SIM systems[7] and has an experimental setup akin to that employed for the generation of complex 3D photonic vortex lattice structures 27 (Fig. 2). In this study, SLM with a high frame rate is used to generate and switch the excitation patterns.

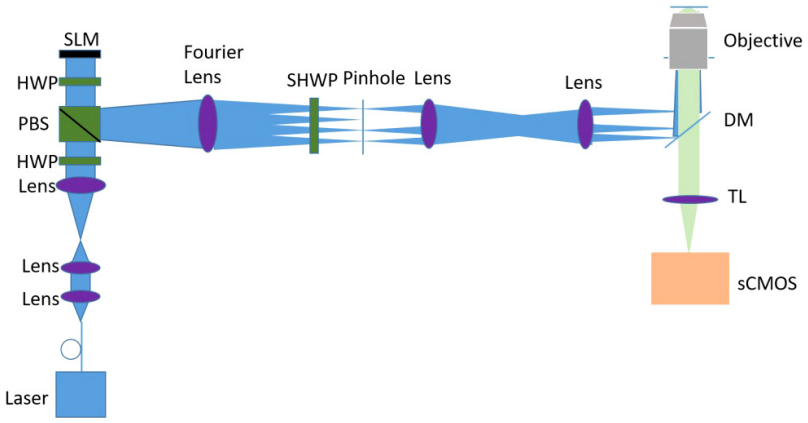

Fig. 2. Simplified diagram of the apparatus: PBS: polarized beam splitting cube; HWP: half-wave plate; SHWP: segmented half-wave plate; BFP: back focal plane; DM: dichroic mirror; TL: tube lens; and sCMOS: scientific CMOS camera.

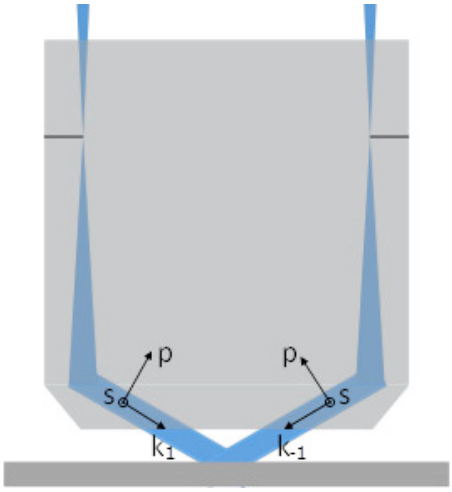

Fig. 3. Schematic diagram of the polarization direction of two beams.

The diffraction orders of +1 and ±2 are filtered out by filter aperture and refocused into the back focal plane of the objective lens. The segmented half-wave plate is disposed behind the filter aperture to adjust the illumination polarization. The objective (60 × PlanApo 1.49NA) collimates the beams and makes them intersect at the focal plane in the sample, where beams interfere with each other to generate an intensity pattern with both axial and lateral structures. An sCMOS camera with 82% peak quantum efficiency is used to detect the emission fluorescence.

3.2. *Polarization modulation method using a segmented half-wave plate*

The illumination intensity distribution on the sample surface in traditional three-beam illumination microscopy can be expressed as follows:

$$I = E_0^2[2 + 2\cos(2k_x x + 2\varphi_n)\cos(\alpha)], \qquad (17)$$

where α denotes the angle between the polarization directions of the illumination light. According to Eq. (17), the contrast of fringe will decrease as α increases. Therefore, it can be predicted that the fringe structure on the sample surface will be blurred when α is large, resulting in greater difficulty in extracting high-frequency illumination.

For a large-numerical-aperture microscopic objective, the angle between the diffraction beams is about 100°, and the beams can be decomposed into the polarization components p (parallel paper surface) and s (vertical paper surface) (see Fig. 3). Since the orientations of the s-polarization components are parallel with each other, the modulation degree of the interference fringes by the s-component is one; meanwhile, the modulation degree of the interference fringes by the p-component is only about 0.17 because the angle between the two p-components of light is 80°. Consequently, the s-component of illumination light on the sample surface should be maintained only to obtain the maximum modulation degree.[28]

In this study, a new method based on a segmented half-wave plate is introduced into the three-dimensional SIM system to modulate the polarized light. The segmented half-wave plate consists of six half-wave plates that have the same area but different fast axis directions [Fig. 4(b)].

Before the polarization modulation, the diffracted beams pass through the $4f$ optical system and the filter apertures that are applied to the formation of the desired +1- and ±2-order diffraction spots. All the diffracted beams in the system have

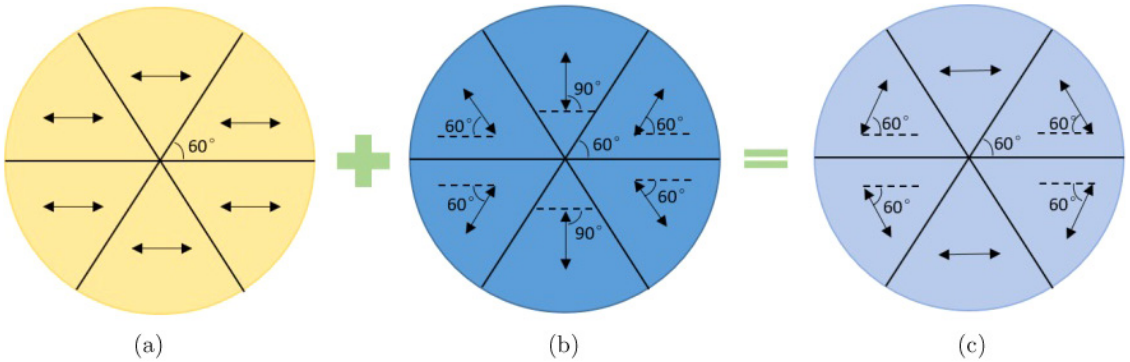

Fig. 4. Schematic diagram of the segmented half-wave plate polarization modulation. (a) Distribution of the incident beam; the arrow indicates the polarization direction of the incident beam. (b) Segmented half-wave plate; the arrow indicates the fast axis direction. (c) Distribution of the outgoing beam on the sample surface; the arrow indicates the polarization direction of the beam.

the same polarization direction [Fig. 4(a)]. The propagation direction of the diffracted beams can be adjusted by controlling the SLM. Moreover, the polarization directions of the incident beams will be modulated to specific directions when they pass through the segmented half-wave plates, as illustrated in Fig. 4(c).

The polarization direction of the beam can always be parallel to the interference fringe direction by using this polarization modulation method. The light on the sample plane has only the s-component, which ensures the maximal fringe modulation degree. There are no moving parts and electro-optic modulation parts in the whole polarization modulation module, resulting in the reduction of time delay for hardware change. The cost of polarization modulation with this method is lower and the imaging performance is more stable compared to the traditional methods.

3.3. *Fast acquisition method of three-dimensional SIM based on asymmetric three-beam interference*

In the system, an SLM was used as a structured light generating device. Due to the working characteristics of the SLM, when it generates the fringe image ($A+$) that we need, it must be accompanied by a loading fringe image ($A-$) with a phase difference of π from $A+$. The fringe image $A-$ shows that we do not need to produce interference fringes, and its loading time is the same as $A+$. For traditional 3D SIM, 15 raw images are required to be taken for each layer of the super-resolution image reconstructed. The time taken by the SLM to load the fringe image $A-$ will be wasted when each raw image is taken. The thicker the sample taken in 3D imaging, the more time wasted.

Different from traditional SIM, it can be deduced from the theory that the interference light I remains unchanged when the phases ϕ_1 and ϕ_2 in Eqs. (2)–(4) change by $\pm\pi$ simultaneously. With the new illumination method, the interference fringe will not change when the phases of the three beams are changed by $\pm\pi$ simultaneously. Therefore, both binary fringes $A+$ and $A-$ loaded by the SLM can be used to produce the same set of illumination stripes. In this study, a unique fast acquisition method is designed by taking advantage of this feature.

As shown in Fig. 5, it is assumed that four raw images need to be collected and the exposure time for acquiring each raw image is 10 ms. The traditional timing acquisition method and the new fast acquisition method we use in our system are illustrated in Figs. 5(a) and 5(b), respectively. The traditional method requires 20-ms acquisition time for each raw image whose exposure time is 10 ms. In the new method we adopted, the fringe images $A+$ and $A-$ generated by the SLM can correspond to the same raw image. The exposure time of the $A+$ and $A-$ stripes is shortened to 5 ms simultaneously, and the images produced by the $A+$ and $A-$ stripes illumination will be both captured by the camera. In this way, the raw image with an exposure time of 10 ms can be captured with an acquisition time of 10 ms. It can be observed that the new acquisition method can reduce the acquisition time of each original image by half.

The raw data of each layer is acquired with seven pattern phases and three pattern orientations with the illumination method based on asymmetric three-beam interference. Specifically, 21 original images are required to reconstruct each layer of super-resolution images. Fifteen raw images are required in traditional three-dimensional SIM. The raw images to be collected are increased from 15 to 21 while the time for acquiring each image is halved; therefore, the time to reconstruct one super-resolution image is reduced by 30%. More time can be saved by using the SIM system based on

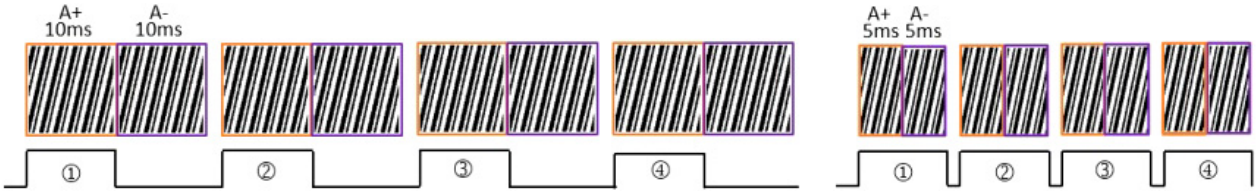

(a) (b)

Fig. 5. (a) Traditional timing acquisition method. (b) New fast timing acquisition method.

asymmetric three-beam interference for three-dimensional imaging. High acquisition speed is significant for avoiding reconstruction artifacts when observing living samples.[22] Therefore, the new SIM with its advantages of fast speed and stability proposed in this study is more suitable for three-dimensional imaging and live-cell imaging.

4. Results and Discussion

In order to quantify the resolution, 100-nm fluorescent microspheres excited by 488-nm laser were constructed. The 3D dataset of 2.5-μm-thick samples was acquired, and the z-step was 0.1 μm. Figures 6(a) and 6(b) show wide-field and SIM results on the 15th xy-plane, respectively. Figures 6(c) and 6(d) show wide-field and SIM results of four beads on the xz-plane, respectively. The light intensity distributions of the fluorescent beads were detected and the full width at half-maximum (FWHM) was determined. As shown in Figs. 6(e) and 6(f), measurements yielded mean FWHMs of 115 nm laterally and 309 nm axially on average for the 3D ATI-SIM. The resolution of the traditional SIM can reach up to 103 nm laterally and up to 279.5 nm axially.[7] Although the requirements for super-resolution imaging have been met, the resolution of ATI-SIM is not as high as that of traditional SIM. However, the stability and speed of three-dimensional imaging will be better than those of a traditional SIM, which will be explained in the second bioimaging example.

Two imaging examples of biological samples with two- and three-dimensional complex structures are illustrated in Figs. 6 and 7 to evaluate ATI-SIM proposed as a good tool for conducting life science research in this study.

For the first biological example, the microtubule cytoskeleton of a HeLa cell was imaged with the single-layer imaging mode of SIM. A 60 × /1.49NA oil immersion objective and 488-nm laser excitation were used. Individual microtubules can be followed.

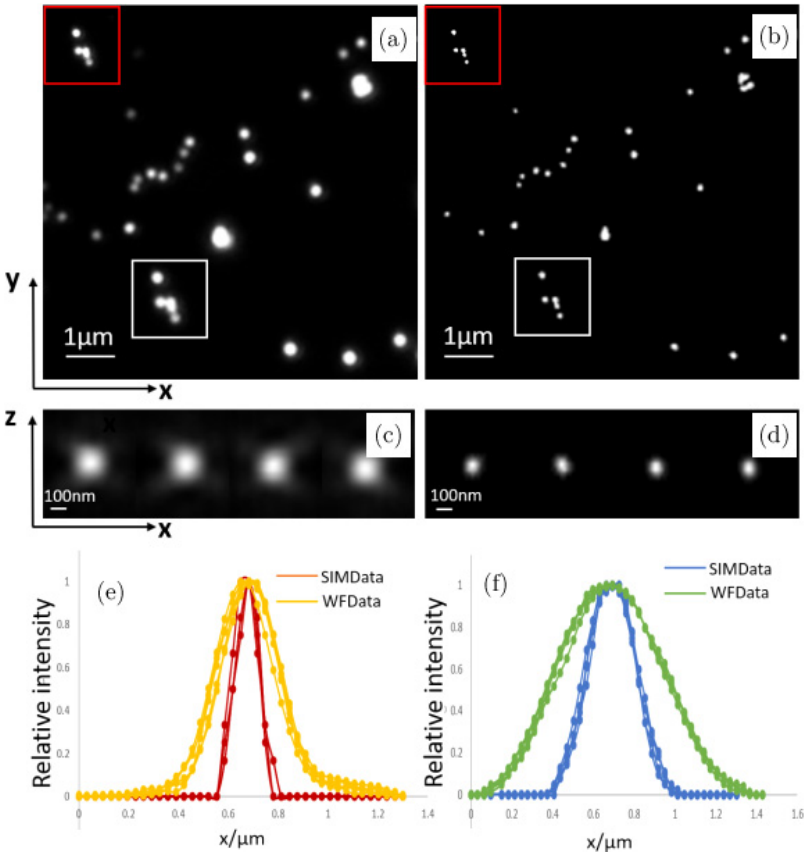

Fig. 6. Experimental reconstruction results of microspheres. (a) Wide-field image of the xy-plane; (b) ATI-SIM image of the xy-plane; (c) wide-field image of the xz-plane; (d) ATI-SIM image of the xz-plane; and (e), (f) four beads' intensity and Gaussian fitting along the lateral and axial directions, respectively.

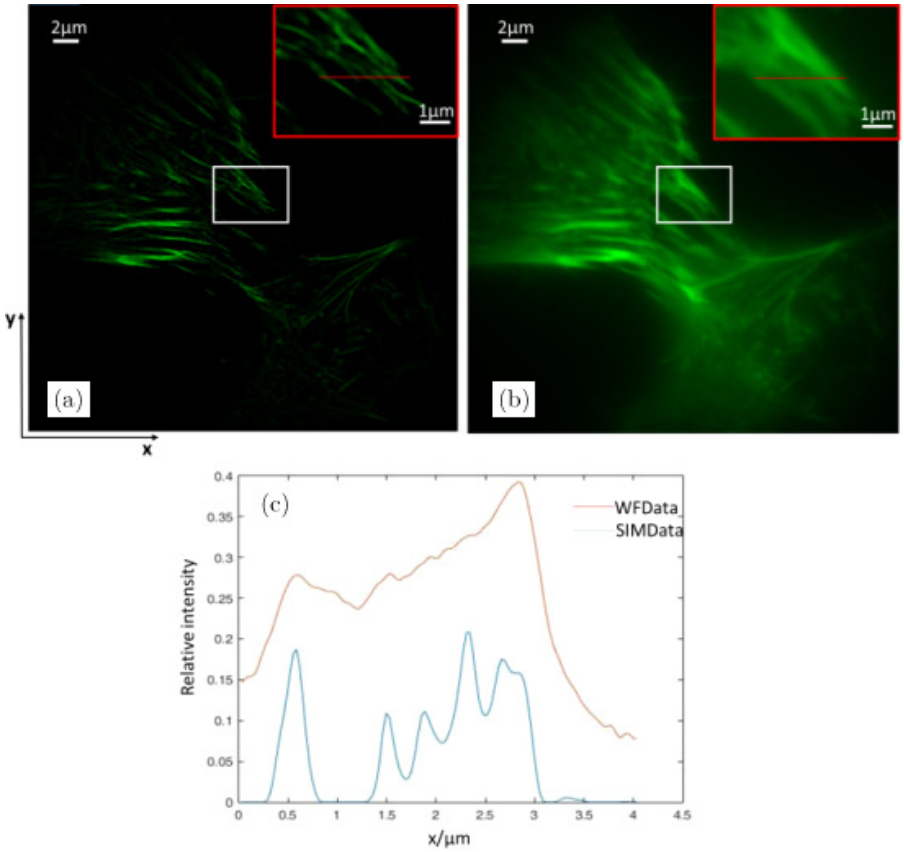

Fig. 7. Experimental results of the microtubule cytoskeleton in the HeLa cell. (a) SIM reconstructed image; (b) wide-field image; and (c) relative intensity of line-scans in (a) and (b). The pictures in the top right corner of each image are local zooms of the red box region.

Three images are presented in Fig. 7. It can be observed in Figs. 7(a) and 7(b) that ATI-SIM produces striking improvements in lateral resolution over the conventional wide-field data, as also verified in Fig. 7(c).

For the second biological example, the Golgi bodies in a mouse kidney section were imaged with the 3D imaging mode. A 60 × /1.49NA oil immersion objective and 488-nm laser excitation were used. Raw data were acquired on 30 z-planes with a 100-nm step. The views of the 17th optical section in the xy-plane obtained by ATI-SIM and wide-field microscopy are illustrated in Figs. 8(a) and 8(b), respectively, while the views of the red line section in the xz-plane are exhibited in Figs. 8(c) and 8(d). The results demonstrate that ATI-SIM produces much-improved lateral and axial resolutions over conventional wide-field microscopy and is indeed able to suppress the out-of-focus blur. Moreover, visualization 1 is the video display of the reconstruction performance of ATI-SIM to offer more intuitionistic information.

Furthermore, the imaging results of the Golgi bodies using the traditional SIM were compared and analyzed to compare ATI-SIM with the traditional SIM based on three-beam interference illumination. Similarly, a 60 × /1.49NA oil immersion objective and 488-nm laser excitation were used. The views of the 25th optical section in the xy-plane obtained by a traditional SIM and a wide-field microscopy are illustrated in Figs. 9(a) and 9(b), respectively, while the views of the red line section in the xz-plane are shown in Figs. 9(c) and 9(d). It can be established through theoretical analysis that the axial resolution of the traditional SIM is higher than that of ATI-SIM. Moreover, although the axial resolution of ATI-SIM is slightly lower, its good performance in experimental studies would not be affected. The 3D dataset of 3-μm-thick samples was acquired and the exposure time of each raw image was 10 ms in both experiments; ATI-SIM only required an acquisition time of 105 ms while the traditional SIM required 150 ms. In our method, the speed was increased by 30%. For three-dimensional imaging or

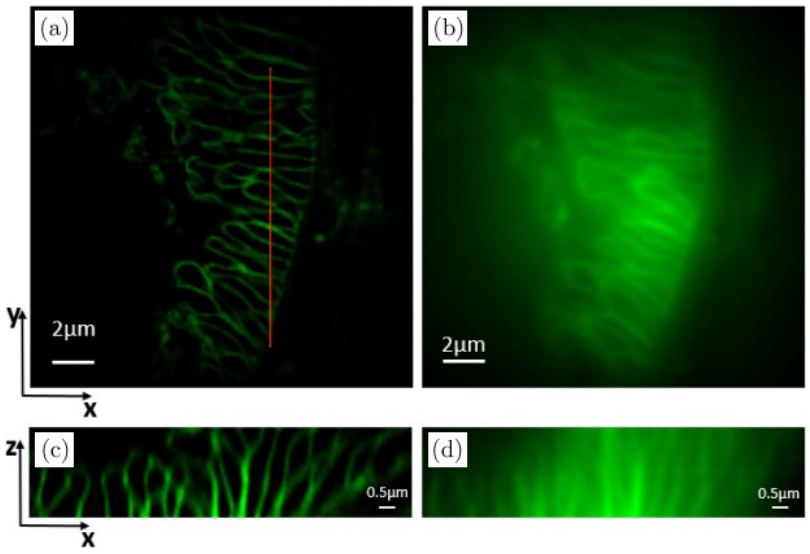

Fig. 8. Experimental results of Golgi bodies in the mouse kidney section. Maximum intensity projection of a SIM z-stack (30 planes, 3-μm thick). (a) SIM reconstructed image in the xy-plane; (b) wide-field image in the xy-plane; (c) SIM reconstructed image in the xz-plane; and (d) wide-field image in the xz-plane.

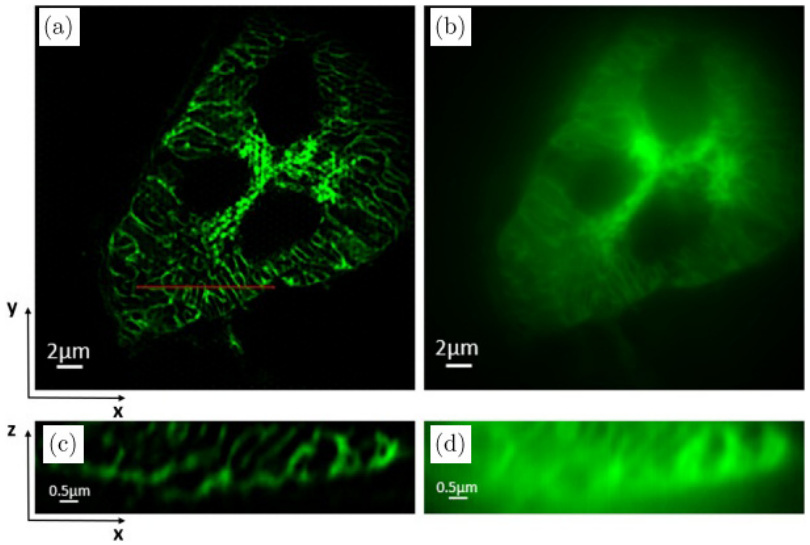

Fig. 9. Experimental results of Golgi bodies. Maximum intensity projection of a SIM z-stack (30 planes, 3-μm thick). (a) SIM reconstructed image in the xy-plane; (b) wide-field image in the xy-plane; (c) SIM reconstructed image in the xz-plane; and (d) wide-field image in the xz-plane.

live-cell imaging, more researchers are paying increased attention to imaging speed.

5. Conclusions and Limitations

In this paper, a novel implementation of SIM based on asymmetric three-beam interference was presented. Different from traditional SIM systems, the illumination light in the proposed system was formed by the interference with +1- and ±2-order diffracted lights. Moreover, the segmented half-wave plate was used to replace the traditional polarization modulation method and was used in a three-dimensional SIM for the first time. Simultaneously, a new acquisition method was adopted due to the characteristics of the new illumination method, contributing to shortening the acquisition time of each raw image by nearly half.

To verify that our system can perform high-quality two- and three-dimensional super-resolution imaging with stable quality, we performed the theoretical derivation of the asymmetric three-beam interference illumination method and imaged the microtubule cytoskeleton of HeLa cell and the Golgi bodies of the mouse kidney section. The experimental results indicate that the system can ensure maximal pattern contrast and long-term stability; meanwhile, imaging resolution in both lateral and axial directions is greatly improved compared with the conventional wide-field microscope. Moreover, the comparison between ATI-SIM and traditional 3D SIM is also performed. Although the axial resolution of ATI-SIM is slightly lower than that of a traditional SIM, the imaging speed is 30% faster. In the fields of three-dimensional morphological imaging of organelles and dynamic imaging of living cells, the imaging speed determines whether a unique research object can be captured. Increasingly more researchers value the three-dimensional imaging speed of super-resolution microscopes, which is also an essential advantage of ATI-SIM.

Thus, ATI-SIM has the advantages of a simple structure, high speed, and good stability. It can be applied to most biomedical research and is especially suitable for fields that require fast 3D imaging and live-cell imaging. In the future, we will develop the technologies of multi-channel and fast three-dimensional living cell imaging based on ATI-SIM, and solve various complications faced by the super-resolution field and the biomedical field.

In this paper, there are still some limitations. How to adjust the light intensities of different diffractive spots to achieve the optimal interference modulation and how to complete the rapid three-dimensional imaging of living cells are our future research focuses.

Conflict of Interest

We declare that we have no financial and personal relationships with other people or organizations that can inappropriately influence our work.

Acknowledgments

This work was funded by The National Key R&D Program of China (2016YFF0102000), Scientific Research and Equipment Development Project of CAS (YJKYYQ20180032 and YJKYYQ20190048), and Major Innovative Research Team of Suzhou (ZXT2019007).

References

1. E. Betzig, G. H. Patterson, R. Sougrat, O. W. Lindwasser, S. Olenych, J. S. Bonifacino, M. W. Davidson, J. Lippincott-Schwartz, H. F. Hess, "Imaging intracellular fluorescent proteins at nanometer resolution," *Science* **313**, 1642–1645 (2006).
2. B. Huang, W. Wang, M. Bates, X. Zhuang, "Three-dimensional super-resolution imaging by stochastic optical reconstruction microscopy," *Science* **319**, 810–813 (2008).
3. M. G. L. Gustafsson, "Surpassing the lateral resolution limit by a factor of two using structured illumination microscopy," *J. Microsc.* **198**(2), 82–87 (2000).
4. R. Heintzmann, C. Cremer, "Laterally modulated excitation microscopy: improvement of resolution by using a diffraction grating," *Proc. SPIE* **3568**, 185–195 (1999).
5. J. T. Frohn, H. F. Knapp, A. Stemmer, "True optical resolution beyond the Rayleigh limit achieved by standing wave illumination," *Proc. Natl. Acad. Sci. USA* **97**, 7232–7236 (2000).
6. M. G. L. Gustafsson, D. A. Agard, J. W. Sedat, "Doubling the lateral resolution of wide-field fluorescence microscopy using structured illumination," *Proc. SPIE* **3919**, 141–150 (2000).
7. M. G. L. Gustafsson, L. Shao, P. M. Carlton, C. J. Wang, I. N. Golubovskaya, W. Z. Cande, D. A. Agard, J. W. Sedat, "Three-dimensional resolution doubling in wide-field fluorescence microscopy by structured illumination," *Biophys. J.* **94**(12), 4957–4970 (2008).
8. S. K. Pal, P. Senthilkumaran, "Cultivation of lemon fields," *Opt. Express* **24**, 28008–28013 (2016).
9. S. K. Pal, Ruchi, P. Senthilkumaran, "C-point and V-point singularity lattice formation and index sign conversion methods," *Opt. Commun.* **393**, 156–168 (2017).
10. S. K. Pal, P. Senthilkumaran, "Lattice of C points at intensity nulls," *Opt. Lett.* **43**(6), 1259–1262 (2018).
11. L. Schermelleh, P. M. Carlton, S. Haase, L. Shao, L. Winoto, P. Kner, B. Burke, M. C. Cardoso, D. A. Agard, M. G. L. Gustafsson, H. Leonhardt, J. W. Sedat, "Subdiffraction multicolor imaging of the nuclear periphery with 3D structured illumination microscopy," *Science* **320**(5881), 1332–1338 (2008).
12. C.-J. R. Wang, P. M. Carlton, I. N. Golubovskaya, W. Z. Cande, "Interlock formation and coiling of

meiotic chromosome axes during synapsis," *Genetics* **183**, 905–915 (2009).
13. V. C. Cogger, G. P. McNerney, T. Nyunt, L. D. DeLeve, P. McCourt, B. Smedsrød, D. G. Le Couteur, T. R. Huser, "Three-dimensional structured illumination microscopy of liver sinusoidal endothelial cell fenestrations," *J. Struct. Biol.* **171**(3), 382–388 (2010).
14. A. C. N. Brown, S. Oddos, I. M. Dobbie, J.-M. Alakoskela, R. M. Parton, P. Eissmann, M. A. A. Neil, C. Dunsby, P. M. W. French, I. Davis, D. M. Davis, "Remodelling of cortical actin where lytic granules dock at Natural Killer cell immune synapses revealed by super-resolution microscopy," *PLoS Biol.* **9**(9), e1001152 (2011).
15. K. F. Sonnen, L. Schermelleh, H. Leonhardt, E. A. Nigg, "3D-structured illumination microscopy provides novel insight into architecture of human centrosomes," *Biol. Open* **1**(10), 965–1041 (2012).
16. J. Tilsner, O. Linnik, M. Louveaux, I. M. Roberts, S. N. Chapman, K. J. Oparka, "Replication and trafficking of a plant virus are coupled at the entrances of plasmodesmata," *J. Cell Biol.* **201**(7), 981–995 (2013).
17. V. W. Rowlett, W. Margolin, "3D-SIM super-resolution of FtsZ and its membrane tethers in Escherichia coli cells," *Biophys. J.* **107**(8), 17–20 (2014).
18. C. Lesterlin, G. Ball, L. Schermelleh, D. J. Sherratt, "RecA bundles mediate homology pairing between distant sisters during DNA break repair," *Nature* **506**(7487), 249–253 (2014).
19. S. T. Ong, G. D. Wright, N. K. Verma, "Three-dimensional structured illumination microscopy (3D-SIM) to dissect signaling cross-talks in motile T-cells," *Methods Mol. Biol.* **1930**, 41–50 (2019).
20. L. J. Young, F. Strohl, C. F. Kaminski, "A guide to structured illumination TIRF microscopy at high speed with multiple colors," *J. Vis. Exp.* **111**, e53988 (2016).
21. L. Shao, E. H. Rego, Structured illumination microscopy, *Fluorescence Microscopy: Super-Resolution and Other Novel Techniques*, A. Cornea, P. M. Conn, Eds., pp. 213–226, Academic Press, Amsterdam (2014).
22. P. Kner, B. B. Chhun, E. R. Griffis, L. Winoto, M. G. L. Gustafsson, "Super-resolution video microscopy of live cells by structured illumination," *Nat. Methods* **6**, 339–342 (2009).
23. R. Förster, H.-W. Lu-Walther, A. Jost, M. Kielhorn, K. Wicker, R. Heintzmann, "Simple structured illumination microscope setup with high acquisition speed by using a spatial light modulator," *Opt. Express* **22**, 20663–20677 (2014).
24. T. Zhao, X. Zhou, D. Dan, J. Qian, Z. Wang, M. Lei, B. Yao, "Polarization control methods in structured illumination microscopy," *Acta Phys. Sin.* **66**, 148704 (2017).
25. G. Machavariani, Y. Lumer, I. Moshe, A. Meir, S. Jackel, "Spatially variable retardation plate for efficient generation of radially and azimuthally polarized beams," *Opt. Commun.* **281**(4), 732–738 (2008).
26. X. Huang, J. Fan, L. Li, H. Liu, R. Wu, Y. Wu, L. Wei, H. Mao, A. Lal, P. Xi, L. Tang, Y. Zhang, Y. Liu, S. Tan, L. Chen, "Fast, long-term, super-resolution imaging with Hessian structured illumination microscopy," *Nat. Biotechnol.* **36**(5), 451–459 (2018).
27. J. Xavier, S. Vyas, P. Senthilkumaran, J. Joseph, "Tailored complex 3D vortex lattice structures by perturbed multiples of three-plane waves," *Appl. Opt.* **51**, 1872–1878 (2012).
28. K. O'Holleran, M. Shaw, "Polarization effects on contrast in structured illumination microscopy," *Opt. Lett.* **22**, 4603–4605 (2012).